The Connectome of a Decision-Making Neural Network

Travis A. Jarrell,[1]* Yi Wang,[1]* Adam E. Bloniarz,[1]† Christopher A. Brittin,[1] Meng Xu,[1] J. Nichol Thomson,[2] Donna G. Albertson,[2]‡ David H. Hall,[3] Scott W. Emmons[1,3]§

In order to understand the nervous system, it is necessary to know the synaptic connections between the neurons, yet to date, only the wiring diagram of the adult hermaphrodite of the nematode *Caenorhabditis elegans* has been determined. Here, we present the wiring diagram of the posterior nervous system of the *C. elegans* adult male, reconstructed from serial electron micrograph sections. This region of the male nervous system contains the sexually dimorphic circuits for mating. The synaptic connections, both chemical and gap junctional, form a neural network with four striking features: multiple, parallel, short synaptic pathways directly connecting sensory neurons to end organs; recurrent and reciprocal connectivity among sensory neurons; modular substructure; and interneurons acting in feedforward loops. These features help to explain how the network robustly and rapidly selects and executes the steps of a behavioral program on the basis of the inputs from multiple sensory neurons.

Animal nervous systems are composed of very large numbers of electrical cells intricately coupled together in complex dynamic networks. Connectionist theories of the nervous system propose that its function is an emergent property of network connectivity. Although the question has been extensively addressed theoretically, the sets of physical connections between neurons within actual nervous systems remain to be described. This is due to the necessity of using electron microscopy (EM) to visualize the subcellular organelles that create the synapses, a technique not amenable to analyzing large structures. To date, the anatomical wiring diagram of only a single animal nervous system has been obtained, that of the adult hermaphrodite of *Caenorhabditis elegans*, published more than 25 years ago (*1*, *2*).

We identified all the chemical and gap junction synapses, the connectome, in the posterior nervous system of the *C. elegans* adult male. This part of the male nervous system contains the circuits and end organs that govern mating behavior (Fig. 1, A and B). In spite of having a relatively simple nervous system, comprising just 302 neurons in the adult hermaphrodite and 383 in the adult male, *C. elegans* expresses a rich and complex behavioral repertoire (*3*, *4*). Many of these behaviors, most notably the sexual behaviors of the male, model the goal-oriented, purposeful activities controlled by decision-making processes characteristic of animal behavior (*5*). The well-fed adult male actively seeks out the hermaphrodite mating partner (*6*–*9*). Physical contact with the hermaphrodite triggers copulation. Copulation consists of a series of stereotyped actions that lead the male to locate the hermaphrodite's vulva, insert its spicules, and transfer sperm (*10*, *11*) (Fig. 1A and movie S1). This multistep behavioral pathway is guided by the activities of 52 sensory neurons located in sexual structures in the tail acting both directly and through interneurons and motorneurons to control 64 muscles and the gonad (Figs. 1B and 2). For success, the male's reactions must be quick (<1 s), because self-fertile *C. elegans* hermaphrodites do not cooperate and may even be resistant to mating (*12*, *13*). The *C. elegans* male posterior nervous system shows how the nervous system evaluates a multiplicity of environmental inputs, makes a rapid behavioral choice, and generates coherent, purposeful behavior.

EM reconstruction of the mating circuits. We determined the male posterior connectome by serial section EM (Fig. 1, C to H) (*14*). The feasibility of comprehensive synapse-level nervous system reconstruction by this method was a primary reason for the initial selection of *C. elegans* as an experimental model (*15*). We developed a PC-based software platform to facilitate assembly of a connectome from electron micrographic images. The connectome is of a single adult animal and was produced from a series of 5000 serial thin sections of 70 to 90 nm encompassing the posterior one-half of the body (fig. S1 and databases S1 to S4) (*16*). It comprises the processes of 170 neurons (89 shared with the hermaphrodite and 81 male-specific) and 64 muscles (24 shared and 40 male-specific) (databases S5 and S6). Among the 170 neurons, 144 lie on synaptic pathways connecting sensory inputs to the end organs involved in mating. These generate the presumptive mating circuits. The remaining 26 neurons, not considered further here, are present in the hermaphrodite as well, with little difference in connectivity and have little or no interaction with male-specific neurons or circuits (database S7).

Properties of the neural network. The 144 neurons, 64 muscles, and gonad that comprise the mating circuits are joined together by both chemical and gap junction synapses (Fig. 3). To analyze this structural network, we took advantage of the mathematical methods of graph theory. If the connectome is considered as a graph, the neurons and muscles are the nodes or vertices. The links or edges connecting vertices represent the total amount of pairwise connectivity resulting from the often multiple (up to 61) separate synapses connecting pairs of cells (fig. S2). Linked vertices are said to be adjacent or neighbors in the graph. In the graph of the male mating circuits, each vertex has multiple neighbors (Fig. 4A). Edges may be directed, if they represent chemical synapses or rectifying gap junctions, or undirected, if they represent nonrectifying gap junctions.

The graph of the connectome may be considered to contain three main subgraphs: (i) a directed graph encompassing the neurons, muscles, and gonad and the chemical connections between them, (ii) a graph of the neurons and their gap junction connections, and (iii) a graph of the muscles and the gap junction connections between them (28 gap junction edges connect neurons to muscles) (Fig. 3). In addition, there are synapses scattered on the hypodermis. Each of the main subgraphs describes a small-world network (*17*). Small-world networks are characterized by having a high value of the clustering coefficient, the probability that, if two vertices are each connected to a common third vertex, then they are connected to each other and, at the same time, low values of the characteristic path length, the average minimum number of edges separating any two vertices. High clustering coefficient suggests local computation, and short path length suggests rapid communication across the network. For the male networks, clustering coefficients are greater than 0.3, and minimum path lengths are <3 steps between pairs of neurons and muscles (table S1). For the entire hermaphrodite chemical network, also a small-world network, the clustering coefficient is 0.22, and the mean path length is 3.48 steps (*2*).

The dynamic properties of a neural network depend on the functional strengths of the synaptic interactions between the cells—in the terms of graph theory, the weights of the edges. To estimate functional strengths from the structure, we judged the physical size of each synapse from the size of the presynaptic density or gap junction

[1]Department of Genetics, Albert Einstein College of Medicine, 1300 Morris Park Avenue, Bronx, NY 10461, USA. [2]Medical Research Council Laboratory of Molecular Biology, Hills Road, Cambridge CB2 0QH, UK. [3]Dominick P. Purpura Department of Neuroscience, Albert Einstein College of Medicine, 1300 Morris Park Avenue, Bronx, NY 10461, USA.

*These authors contributed equally to this work.
†Present address: Department of Statistics, University of California, Berkeley, Berkeley, CA 94720, USA.
‡Present address: Helen Diller Family Comprehensive Cancer Center, University of California, San Francisco, 1450 Third Street, San Francisco, CA 94158, USA.
§To whom correspondence should be addressed. E-mail: scott.emmons@einstein.yu.edu

structure and summed over all the synapses between each pair of cells (*16*). (The resulting structural weight adjacency matrices for the chemical and gap junction networks are given as databases S8 and S9). Individual presynaptic densities varied in size over a 40-fold range, whereas individual gap junctions varied in size over a 30-fold range (fig. S2). As a result of the variation in both number of synapses between pairs

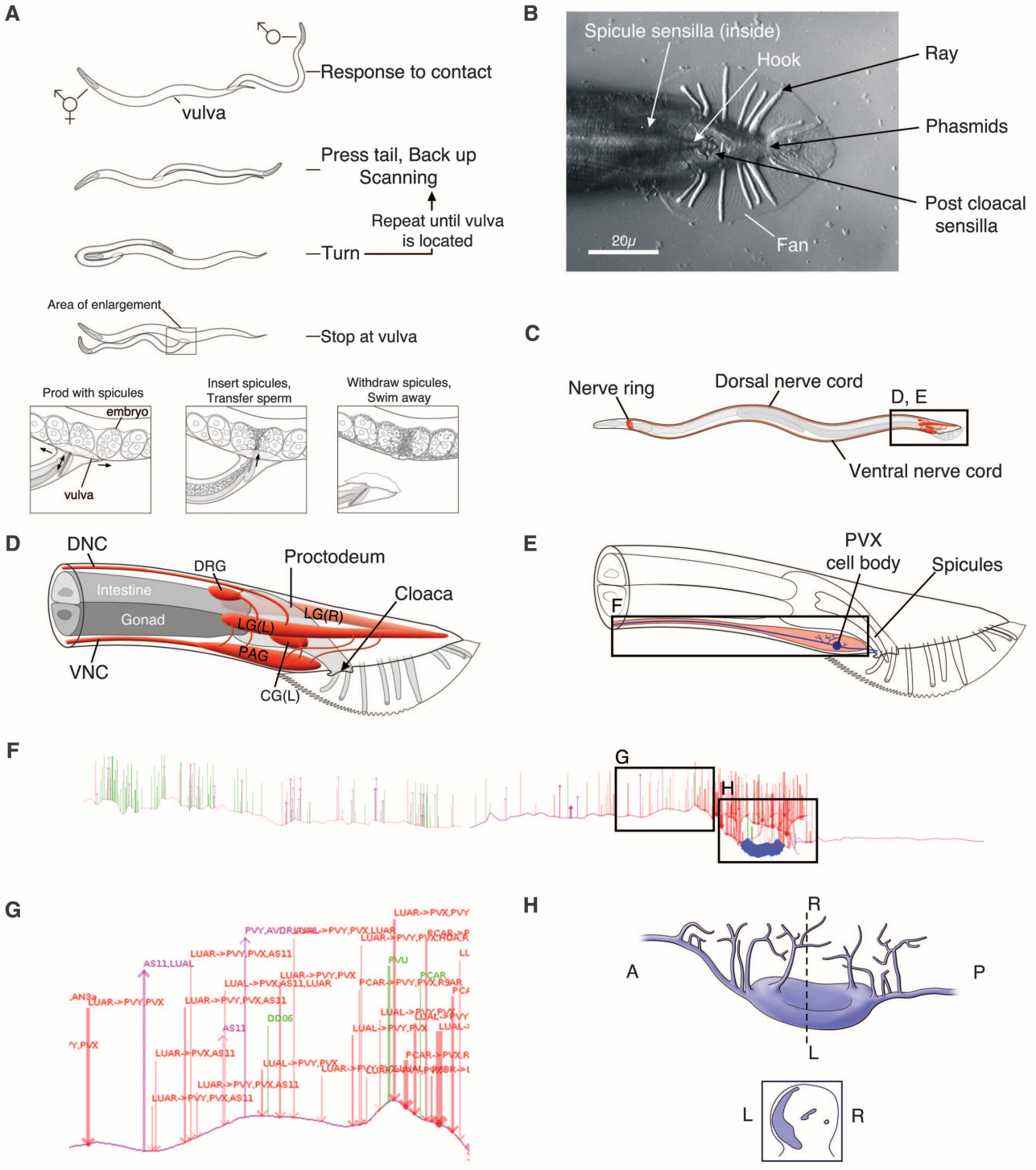

Fig. 1. Specializations of the *C. elegans* adult male tail for mating. (**A**) The substeps of mating. (**B**) Ventral view of the adult male tail showing mating structures with five types of sensilla. (**C**) Overall structure of the male nervous system. (**D**) Ganglia in the tail containing the neuron cell bodies, connected through commissures. Most synaptic connectivity occurs in the preanal ganglion (PAG). DNC, dorsal nerve cord; VNC, ventral nerve cord; DRG, dorsorectal ganglion; LG, lumbar ganglion (left and right); CG, cloacal ganglion (left and right). (**E**) An example of a male-specific interneuron, PVX, which has a cell body and extensive sensory input in the PAG, and a process extending into the VNC, where there is output onto motorneurons and muscles. (**F**) Overall structure of PVX showing distribution of synapses (dorsal view). Red: chemical input; magenta: chemical output; green: gap junction. (**G**) Detail of individual synapses showing synaptic partners. Many chemical synapses are dyadic or polyadic. Width of lines indicates synapse size. Intermingling of input and output is consistent with PVX being a graded potential neuron (*46*). (**H**) Branching structure around the PVX cell body (dorsal view). The cell body forms a crescent shape lying against the basement membrane surrounding the PAG (transverse section in inset).

A
MUSCLES THAT BEND THE BODY
aol: anterior outer longitudinals; dBWM: dorsal body wall muscles; pol: posterior outer longitudinals; cdl: caudal longitudinals; vBWM: ventral body wall muscles; dgl: diagonal muscles; ail: anterior inner longitudinals; pil: posterior inner longitudinals

B
MUSCLES THAT CONTROL THE CLOACAL OPENING AND SPICULES
dsr: dorsal spicule retractor; dsp: dorsal spicule protractor; gec: gubernacular erector; grt: gubernacular retractor; aob: anterior oblique; pob: posterior oblique; vsp: ventral spicule protractor; vsr: ventral spicule retractor; adp: anal depressor

C
RESPONSE MODULE
sensory neurons: PHAL, PHAR, PHBL, PHBR, R2BL, R2BR, R3BR, R4BL, R4BR, R8AL, R8AR, R8BL, R9AL, R9AR, HOA, PCAL, PCAR, AVG
interneurons: PVY, PVX, LUAL, LUAR, DX1, DX3, CA07, PVNL, PVZ, AVBR
motor neurons: DA04

LOCOMOTION MODULE
sensory neurons: SPDL, SPDR, SPVL, SPVR
interneurons: AVAL, AVAR, AVBL, AVDL. AVDR, PVCL, PVCR, CA08, DVC, PVU
motor neurons: DA07, DA08, DA09, DB05, DD03, DD06, VA09, VA10, VA11, VA12, VB05, VB06, VB07, VB08, VB09, VB10, VB11, VD09, VD10, VD11, VD12, DA05, DA06, DB04, DB06, DB07, DD04, DD05, AS08, AS09, AS10
muscle groups: vBWM, ail/pil

D
R(1-5)A MODULE
sensory neurons: R1AL, R1AR, R2AL, R2AR, R3AL, R3AR, R4AL, R4AR, R5AL, R5AR, CA09
muscle groups: dgl, cdl/pol

E
PVV MODULE
sensory neurons: R1BL, R1BR, R3BL,R5BL, R5BR, R6AL, R6AR, R6BL, R6BR, R7AL, R7AR, R7BL, R7BR, R9BL, R9BR
interneurons: CP07, CP08, CP09, PDA, PDB, PDC, PVV, CA04, PGA, AN3a, AN3b, PVNR
motor neurons: AS11, VD13, PVS
muscle group: dBWM

F
INSEMINATION MODULE
sensory neurons: HOB, PCBL, PCBR, PCCL, SPCL, SPCR
interneurons: AVL, DX2, CA02, CA03, CA05, CA06, CP01, CP02, CP03, CP04, CP05, CP06, DVB, DVE, DVF, PVT
muscle groups: sph, grt/gec/aob/pob, vsp/dsp/adp, int
gonad

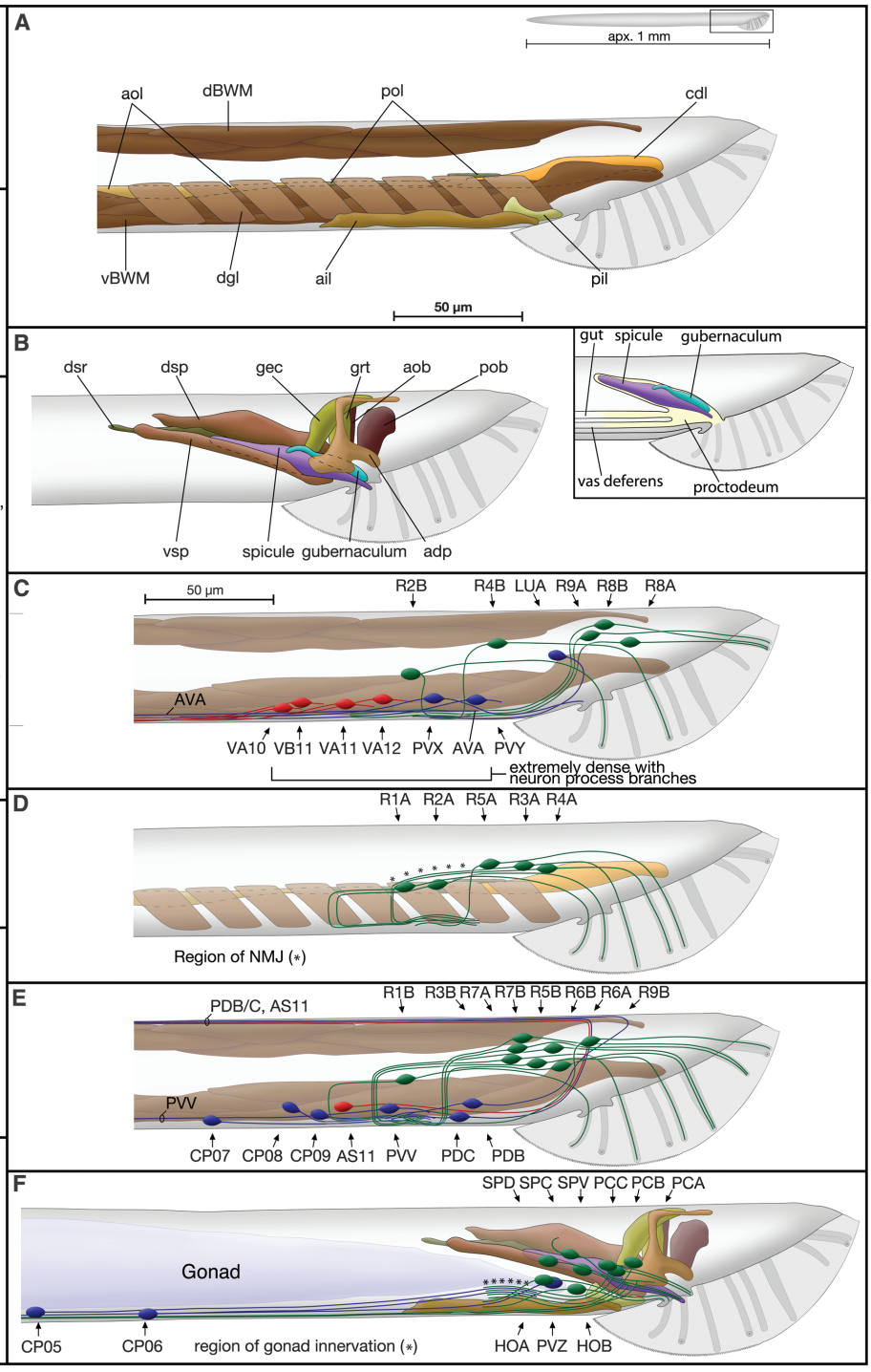

Fig. 2. The neurons and muscles of the mating circuits. (**A**) and (**B**) show the muscles. (C to F) The left column lists the neurons and muscles grouped into mathematically defined "modules" on the basis of their connectivity that match elements of mating behavior (Fig. 1A); the right column illustrates the locations of the cell bodies and processes of the key neurons in each module together with the muscles that are targeted (sensory neurons: green; interneurons: blue; motor neurons: red). (**C**) Response and Locomotion modules. The key sensory input to the Response module is from the B-type neurons of the subset of rays with openings on the ventral side of the fan, rays 2, 4, and 8. The dendritic endings of these neurons will be in contact with the hermaphrodite body when the male is correctly oriented to mate. Experimental evidence indicates that the B-type ray neurons promote the Response step (*21, 26*). The Response module drives the Locomotion module, containing body-wall motor neurons, via the command interneurons. (**D**) R(1-5)A module. Neuromuscular junctions of the A-type ray neurons onto the diagonal and longitudinal muscles are consistent with experimental evidence for a role of these sensory neurons in promoting ventral curling of the tail during mating (*25*). (**E**) PVV module. This module, so-named for the large, male-specific PVV interneuron, has output onto the ventral body-wall motor system, via PVV, and onto the dorsal body-wall muscles, via PDA, PDB, PDC, and AS11. The dual innervation of both dorsal and ventral gender-shared body-wall muscles, mostly bypassing the command interneurons, suggests that this module, like the R(1-5)A module, is involved in aspects of male posture during mating (*47*). (**F**) Insemination module. This module will take over the male's behavior once the vulva is sensed. All the neurons involved in insemination are shown here, although PCA, owing to its strong connection to PVX; HOA, owing to its connection to LUA; and PVZ, owing to its connection to HOA are all in the Response module, whereas SPD, because of its muscle output, and SPV, because of its connection to SPD, are in the Locomotion module (see Fig. 6).

of cells and sizes of individual synapses, total morphometric connectivity weights vary more than 100-fold and cover a continuous range of values (Fig. 4B). Each neuron has both strong and weak synaptic partners (Fig. 4C). Structural weights are likely to be related to the functional strengths of the synaptic interactions (*18*), but the signs of the chemical interactions, that is whether a given synapse is excitatory or inhibitory, cannot be determined from the electron micrographs.

We next asked whether all of the interactions, including the large number of weak interactions, are likely to be significant to network function. Weak connections (chemical connections of less than 20 sections and gap junction connections of less than 16 sections) carried half the load through the respective graphs (Fig. 4D). For both chemical and gap junction networks, left-right homologs—presumptively equivalent cells—had similar sets of synaptic partners, and this was true even when only the connections in their weaker set were compared (fig. S3) (*16*). Therefore, at least some of the weaker connections are not random. For the purpose of exploring network structure, we have included all synaptic interactions in our analysis.

Information flow through the network. With the morphological sizes of the physical connections serving as proxies for functional synaptic strengths, the weight adjacency matrices allow us to trace a hypothetical overall information flow through the network from sensory input to end-organ output (Fig. 5A). Much of this information flow is through monosynaptic pathways. Fifty-five percent of the input to the motor system (muscles, body-wall motor neurons, and command interneurons) comes directly from sensory neurons, including 45% of the input to the muscles themselves. Similarly, 76% of the input to the gonad comes directly from sensory neurons and is expected to control outflow of sperm during mating. The remaining input to the motor system and gonad comes from a subset of 32 neurons that we classify as interneurons because they have considerable output onto other neurons, including motor neurons, but some of them also form neuromuscular junctions and, hence, have motor neuron character as well (databases S8 and S9). Because these interneurons all receive sensory input, much of the remaining information flow to the end organs is through disynaptic pathways, and the network has an overall feedforward-loop architecture. The virtual absence of neural feedback from the end organs means that it is the physical output of the system—the male's motion with respect to the hermaphrodite and sperm transfer—that feeds back to the sensory inputs to provide control to the network.

In addition to the interneurons that participate locally in the mating circuits, which we term type I interneurons, a second class of 12 interneurons (type II interneurons) interacts with neurons and end organs in the mating circuits and, in addition, they have a process extending through the ventral nerve cord and into the nerve ring, where they presumably interact with the anterior nervous system through connections that are yet to be determined. Type II interneurons are likely to play a role in coordinating mating with other behavioral programs. In support of this conclusion, the mate-searching behavioral state, which is stimulated by the male rays, requires communication to the anterior through three male-specific type II interneurons—EF1, EF2, and EF3—which receive extensive input from sensory neurons, particularly B-type ray sensory neurons (*8*). In the posterior circuits, type II interneurons interact (both input and output) primarily with sensory neurons and, to a lesser extent, with the type I interneurons.

The locally acting type I interneurons can be further subdivided into three subtypes based on the nature of their primary postsynaptic targets (Fig. 5, B and C). Type Ia, consisting of 14 neurons in six classes, has output primarily onto the end organs—elements of the motor system or the gonad or both. Information flow through the Ia interneurons is strongly feedforward. Type Ib, consisting of 10 neurons in three classes, has output primarily onto type Ia interneurons and also has feedback onto sensory neurons. Type Ic, consisting of seven neurons in two classes, is connected to sensory neurons, type Ia interneurons, and end organs (the spicule muscles) in such a way as to suggest that this class of interneurons mediates ending mating or moving the program to an earlier step (supplementary text and fig. S11).

Network community structure identifies subcircuits for separate functions in mating. To map the behavioral program for mating onto the connectome and to ask whether each substep has a dedicated neural substrate, we examined the network for modular architecture (*19*). Modules or communities in a graph are subsets of vertices more strongly connected to each other than to vertices in other communities. Using the spectral method (*20*) for optimal network partitioning, we found that the network could be partitioned with high statistical significance into five meaningful communities (modularity coefficient $Q = 0.451$; $P < 10^{-7}$) (Fig. 2) (*16*). Other methods for graph partitioning gave similar results (supplementary text). These communities placed the sensory neurons into coherent receptive fields. The neurons and end organs suggest that they contain subcircuits dedicated, respectively, to the search for the vulva [Response step (*21*)], locomotion, posture (two communities), and insemination. These functional assignments and the cellular composition of

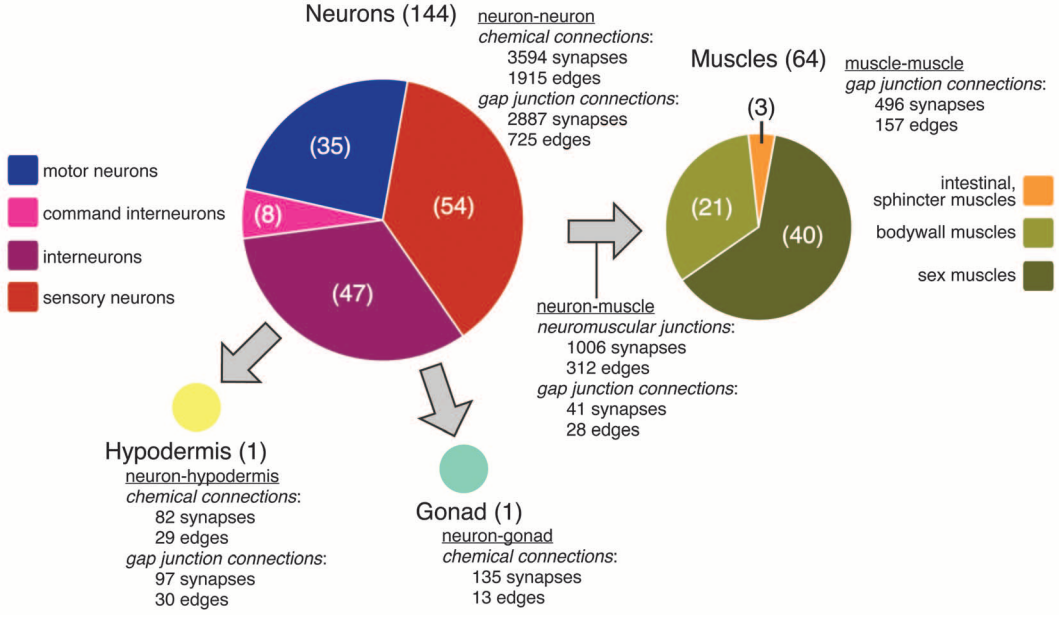

Fig. 3. Total numbers of vertices (numbers in parentheses), synapses, and edges in the subgraphs of the posterior connectome. For comparison, the graph of neuron-to-neuron connections for the entire hermaphrodite nervous system (excluding the 20 neurons of the pharyngeal nervous system) has 279 vertices (neurons), 2194 directed chemical edges, and 514 gap junction edges (*2*). The numbers of chemical and gap junction edges in the subgraph of neuron-to-neuron connections are, respectively, 11% and 10% of the total number of possible edges among the 144 neurons.

each module correlate well with experimental evidence (*21*–*26*).

Sensory neurons are recurrently connected. Whereas much of the information flow through the network from sensory neurons to end organs—either in monosynaptic pathways or through type Ia interneurons in disynaptic pathways—is feedforward, the 52 sensory neurons are extensively reciprocally and recurrently connected by both chemical and gap junction synapses. Forty-nine percent of the chemical synaptic output of sensory neurons is onto other sensory neurons, and this constitutes input to the sensory neurons that is seven times the feedback from type Ib and type Ic interneurons. Nineteen out of the 36 ray sensory neurons make autapses, constituting 6.9% of their input from sensory neurons. Fifty-eight percent of the gap junction connectivity of the sensory neurons is with other sensory neurons.

Only on the basis of the recurrent connectivity of the sensory neurons and their connections to the type Ib interneurons, the network of sensory neurons could be partitioned into a set of modules similar to those of the entire network (supplementary text) (fig. S6). Recurrent and reciprocal connectivity of sensory neurons is expected to amplify input signals through loop gain. Recurrent dynamic networks may exhibit fixed point or attractor behavior characterized by feedback-reinforced stable modes of network activity (*27*, *28*). Modularity at the level of the sensory neurons suggests that sensory input may drive the network into discrete modes of self-reinforcing activity, each associated with one aspect or substep of the mating program (*29*, *30*).

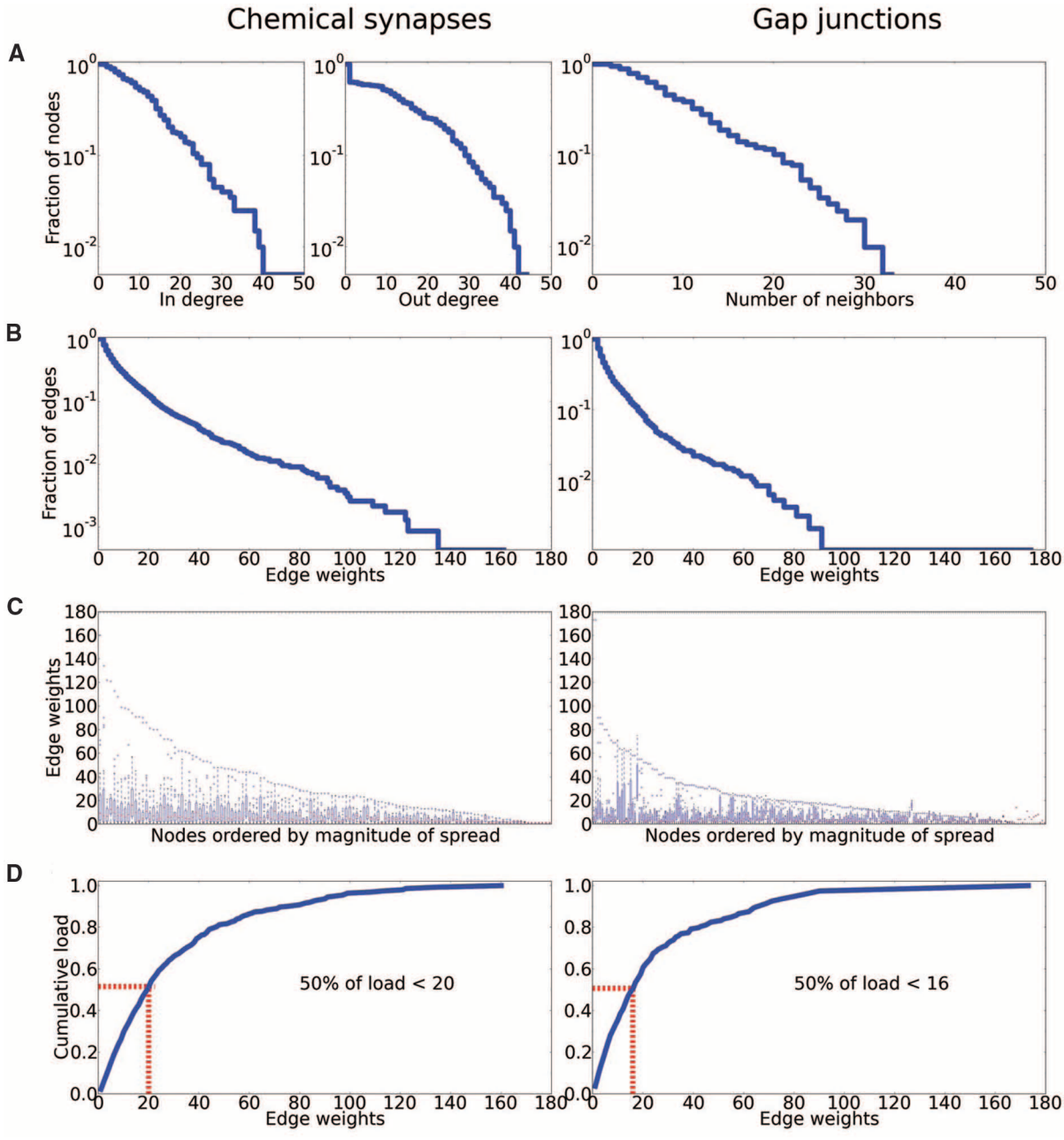

Fig. 4. Network properties of the connectome. (**A**) Degree (neighbor) distributions (number of edges for each vertex) in the chemical and gap junction networks (survival function). (**B**) Distributions of the edge weights (survival function). Edge weights are determined by counting the number of 70- to 90-nm serial sections crossed by individual synapses and summing over all the synapses between pairs of neurons and muscles. (**C**) Each neuron has a range of stronger and weaker synaptic partners. Points on the abscissa give the strengths of the individual edges of a given vertex. (**D**) Distribution of cumulative load versus edge weight. Weak connections carry a significant fraction of the load through the network.

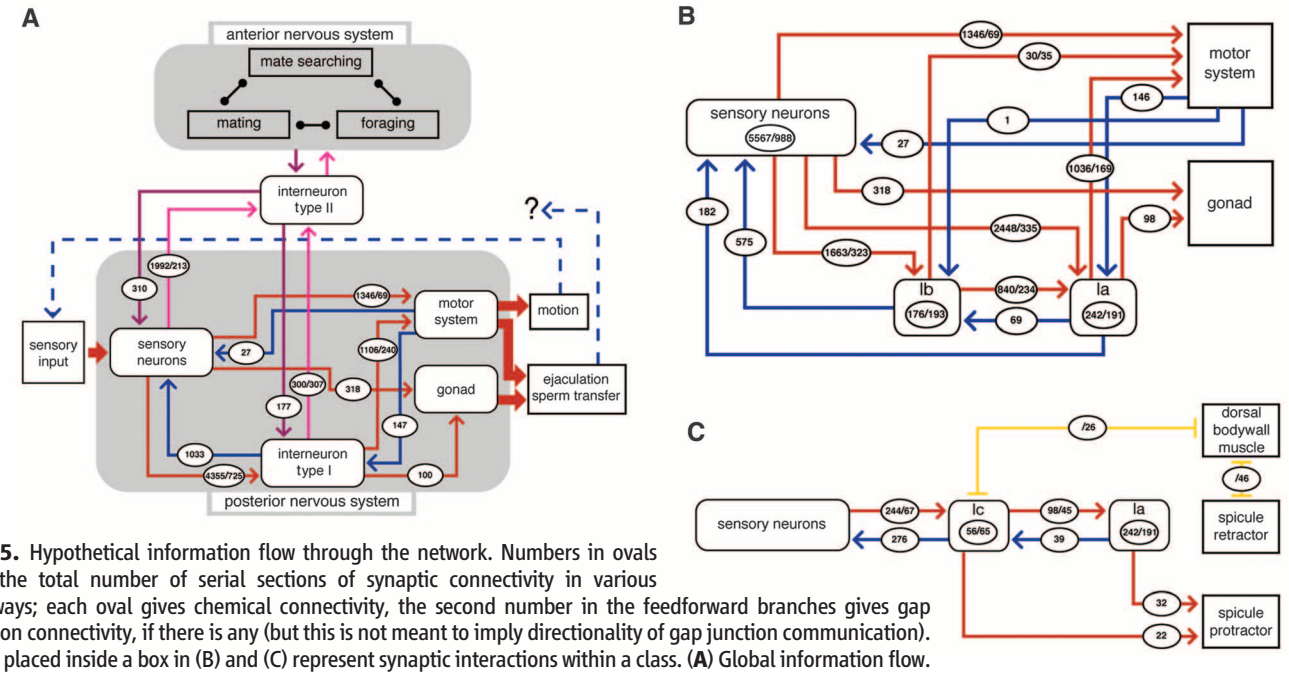

Fig. 5. Hypothetical information flow through the network. Numbers in ovals give the total number of serial sections of synaptic connectivity in various pathways; each oval gives chemical connectivity, the second number in the feedforward branches gives gap junction connectivity, if there is any (but this is not meant to imply directionality of gap junction communication). Ovals placed inside a box in (B) and (C) represent synaptic interactions within a class. (**A**) Global information flow. Information flow between sensory neurons and end organs is both direct in monosynaptic pathways and via interneurons. A second class of interneurons communicates to the head. (**B**) Two layers of interneurons convey information to the end organs. Information flow through the type Ia layer is almost exclusively feedforward. (**C**) A third class of interneurons has feedback onto sensory neurons and output onto elements of the ejaculatory circuits, including the spicule muscles, which suggests that this class is involved in ending mating (see supplementary materials for greater detail of the type Ic circuits).

Information flow through interneurons creates feedforward loops. The male mating circuits have a statistically high frequency of feedforward loops (fig. S10). Examination of the feedforward circuits through the Ia and Ib interneurons reveals that these circuits are loops in which, for each interneuron class, input sources and output targets are themselves connected (Fig. 6A). At a finer level of detail, Fig. 6B illustrates this role of the CP(01-06) class in the Insemination module.

The function of a feedforward loop depends on whether the net signs of the two branches are the same (coherent feedforward loop) or opposite (incoherent feedforward loop) (*31*, *32*). Because the targets receiving input from CP(01-06) would all seem to function together during insemination behavior at the vulva, it appears most likely that the feedforward loops created by the CP(01-06) class are coherent feedforward loops. They pool sensory inputs and may serve to coordinate the actions of end organs that individually receive much of their input from different sets of sensory neurons. Their activity may, in addition, reinforce and sustain the activity within the insemination module. As a similar logic can be applied to the other feedforward loops in the network, each may be a coherent feedforward loop. Coordination and reinforcement of functional pathways that receive multiple sensory inputs and have multiple end-organ targets may be the general function of interneurons and this circuit motif here.

Conclusion. Mating is typically a complex behavior essential for the survival of most species. In the *C. elegans* male, enlargement of the posterior nervous system in support of this behavior adds some 30% more neurons and complex connectivity equal to that of the entire hermaphrodite nervous system. Connectomics emphasizes the importance of a complete, synapse-level structural description of the nervous system for understanding nervous system function (*33*–*39*). Our structural analysis allowed us to define the neural substrate for mating behavior, to identify classes of neurons and assign functions to them, and to suggest how the topology of the network of connections contributes to the control of behavioral output.

The brain performs certain types of computations far faster, more robustly, and with much less power consumption than digital computers based on semiconductors and Von Neumann architecture (*27*, *40*). Parallel distributed processing and recurrent connectivity are thought to provide part of the explanation for these properties. Both of these structural principles are present in the *C. elegans* male mating neural network. Sensory information is aggregated at three levels through the network—at the level of recurrent connectivity among the sensory neurons; at the end organs, which receive direct sensory input from multiple sensory neurons; and at the interneurons. Information flow to each end organ through many parallel pathways will ensure network robustness. Recurrent connectivity among the sensory neurons and between sensory neurons and the type Ib interneurons suggests that, at these levels, the network could have so-called attractor dynamics. Attractor dynamics are characterized by abrupt transitions between self-reinforcing stable modes of network activity (*41*–*43*). Such rapid shifts in behavior are observed in *C. elegans* male mating. If the male mating network exhibits attractor dynamics, then, as a transition in network output occurs as a direct result of a change in sensory input, decision-making and behavioral switching are one and the same event. In this way, the structure could provide economy and efficiency. In contrast to the recurrent connectivity of the sensory neurons, aggregation of sensory information at the level of the type Ia and Ib interneurons in feedforward pathways suggests the architecture of a perceptron (*44*). Indeed, the system may be considered to solve a pattern recognition or classification problem, where the male attempts to interpret correctly its position with respect to the hermaphrodite.

The set of activity weights in an adjacency matrix of a neural network, upon which the network's input-output function in part depends, may be considered the network's "knowledge" about its environment (*45*). Because *C. elegans* male mating is an innate behavior, the weights in the mating neural network, both physical, as measured here, and functional, are genetically specified. Genetic specification is evident in the reproducibility of the connectivity of presumptively equivalent neurons, such as left-right homologs, as well as in the sexual dimorphism of certain shared neurons (sexual phenotype is thought to be cell-autonomous in *C. elegans*). Because the network's structure is genetically encoded, the learning algorithm by which this

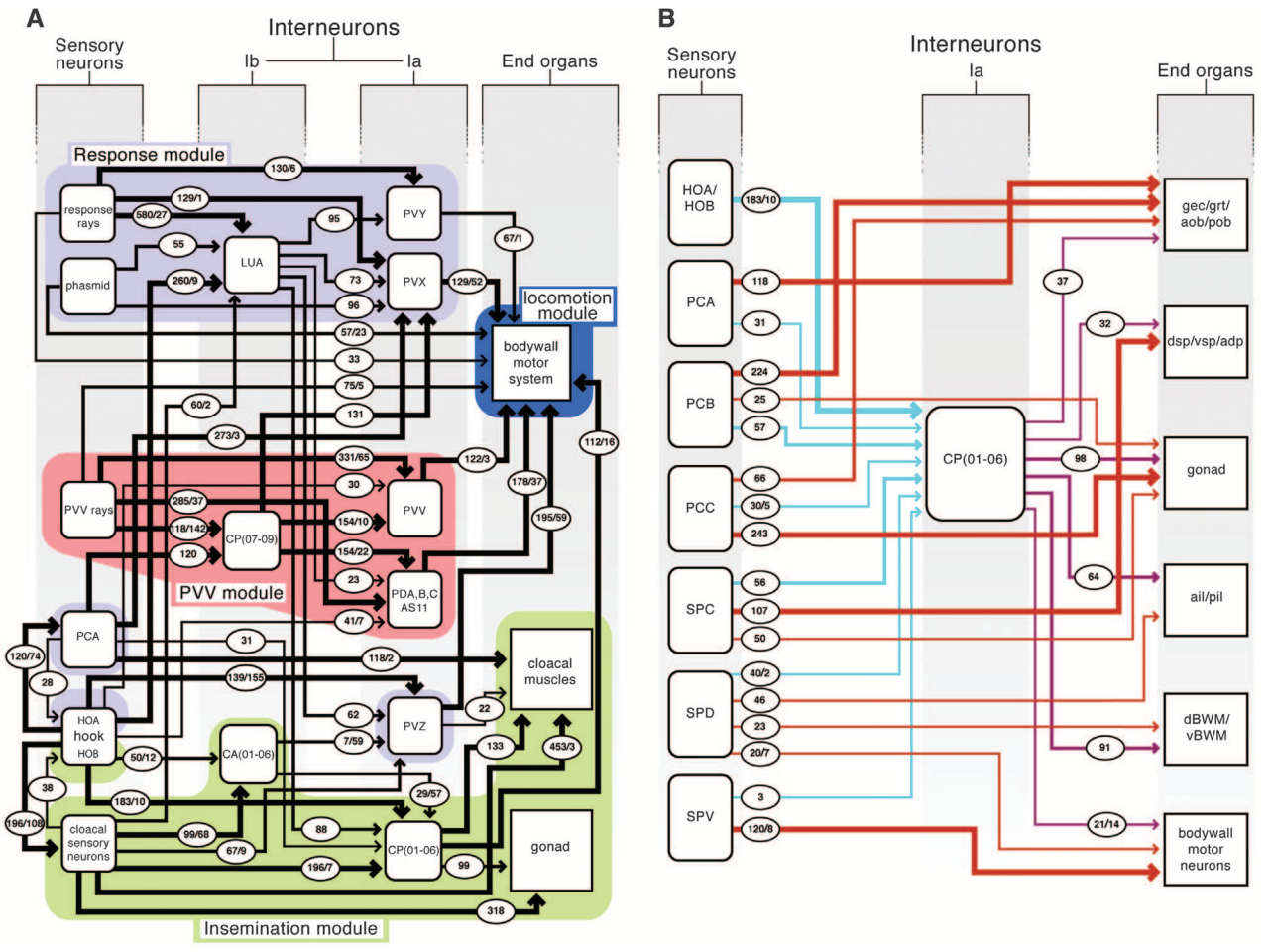

Fig. 6. The feedforward circuits through the modules. Numbers in ovals as for Fig. 5. [The R(1-5)A module is omitted.] (**A**) The Response, PVV, and Insemination modules each contain a subset of type Ia interneurons and one class of type Ib interneuron. All interneuron classes participate in feedforward loops, type Ia targeting end organs, type Ib targeting type Ia. Cross connections between the modules are created at the level of the type Ib interneurons. Among sensory neurons, the hook neurons are distinctive in not having any direct output onto end organs and in having strong output onto other classes of sensory neurons, namely, the neurons located in the postcloacal sensilla and the spicules. (The many other cross-connections between sensory neurons are not shown.) PCA is separated out from the other cloacal sensory neurons to show its feedforward loop involving CP(07-09) and PVX. LUA(L/R), PDA, PDB, and AS11 are shared neurons that are sexually dimorphic. (**B**) Greater detail of the feedforward loops in the insemination circuits through the CP(01-06) interneuron class.

knowledge has been acquired is natural selection. The structural design must be fault-tolerant in order to allow for developmental error. The continuous distribution of connection strengths in the male posterior connectome suggests a probabilistic mechanism of synapse formation in which each cell pair has a genetically specified probability of forming a synapse. Small evolutionary changes in these probabilities will allow gradual evolution of structural connectivity and hence of network function and behavior.

References and Notes

1. J. G. White, E. Southgate, J. N. Thomson, S. Brenner, *Philos. Trans. R. Soc. Lond. B Biol. Sci.* **314**, 1 (1986).
2. L. R. Varshney, B. L. Chen, E. Paniagua, D. H. Hall, D. B. Chklovskii, *PLOS Comput. Biol.* **7**, e1001066 (2011).
3. M. de Bono, A. V. Maricq, *Annu. Rev. Neurosci.* **28**, 451 (2005).
4. M. de Bono, M. B. Sokolowski, in *Invertebrate Neurobiology,* G. North, R. J. Greenspan, Eds. (Cold Spring Harbor Laboratory Press, Cold Spring Harbor, NY, 2007).
5. X.-J. Wang, *Neuron* **60**, 215 (2008).
6. J. Lipton, G. Kleemann, R. Ghosh, R. Lints, S. W. Emmons, *J. Neurosci.* **24**, 7427 (2004).
7. J. M. Simon, P. W. Sternberg, *Proc. Natl. Acad. Sci. U.S.A.* **99**, 1598 (2002).
8. A. Barrios, S. Nurrish, S. W. Emmons, *Curr. Biol.* **18**, 1865 (2008).
9. J. Q. White *et al.*, *Curr. Biol.* **17**, 1847 (2007).
10. J. E. Sulston, D. G. Albertson, J. N. Thomson, *Dev. Biol.* **78**, 542 (1980).
11. M. M. Barr, L. R. Garcia, in Neurobiology and behavior section, E. M. Jorgensen, J. M. Kaplan, Eds., *WormBook* (The *C. elegans* Research Community, WormBook, 2006); www.wormbook.org/toc_complete.html
12. L. R. Garcia, B. LeBoeuf, P. Koo, *Genetics* **175**, 1761 (2007).
13. G. A. Kleemann, A. L. Basolo, *Anim. Behav.* **74**, 1339 (2007).
14. Neuron maps, synapse lists, and connectivity matrices are available at http://wormwiring.org.
15. S. Brenner, *Genetics* **77**, 71 (1974).
16. Materials and methods are available as supplementary materials on *Science* Online.
17. D. J. Watts, S. H. Strogatz, *Nature* **393**, 440 (1998).
18. T. Schikorski, C. F. Stevens, *J. Neurosci.* **17**, 5858 (1997).
19. M. E. J. Newman, *Proc. Natl. Acad. Sci. U.S.A.* **103**, 8577 (2006).
20. E. A. Leicht, M. E. J. Newman, *Phys. Rev. Lett.* **100**, 118703 (2008).
21. K. S. Liu, P. W. Sternberg, *Neuron* **14**, 79 (1995).
22. K. Liu, Ph.D. thesis, California Institute of Technology (1995).
23. L. R. Garcia, P. Mehta, P. W. Sternberg, *Cell* **107**, 777 (2001).
24. Y. Liu *et al.*, *PLoS Genet.* **7**, e1001326 (2011).
25. P. K. Koo, X. Bian, A. L. Sherlekar, M. R. Bunkers, R. Lints, *J. Neurosci.* **31**, 7497 (2011).
26. M. M. Barr, P. W. Sternberg, *Nature* **401**, 386 (1999).
27. J. Hertz, A. Krogh, R. G. Palmer, *Introduction to the Theory of Neural Computation, Santa Fe Institute Studies in the Sciences of Complexity* (Westview Press, Boulder, CO, 1991).
28. J. J. Hopfield, *Proc. Natl. Acad. Sci. U.S.A.* **79**, 2554 (1982).
29. D. Kleinfeld, *Proc. Natl. Acad. Sci. U.S.A.* **83**, 9469 (1986).
30. D. Kleinfeld, H. Sompolinsky, *Biophys. J.* **54**, 1039 (1988).
31. S. Mangan, U. Alon, *Proc. Natl. Acad. Sci. U.S.A.* **100**, 11980 (2003).
32. U. Alon, *Nat. Rev. Genet.* **8**, 450 (2007).
33. H. S. Seung, *Neuron* **62**, 17 (2009).
34. O. Sporns, G. Tononi, R. Kötter, *PLOS Comput. Biol.* **1**, e42 (2005).
35. J. W. Lichtman, J. R. Sanes, *Curr. Opin. Neurobiol.* **18**, 346 (2008).
36. Y. Mishchenko *et al.*, *Neuron* **67**, 1009 (2010).

37. D. D. Bock *et al*., *Nature* **471**, 177 (2011).
38. K. L. Briggman, M. Helmstaedter, W. Denk, *Nature* **471**, 183 (2011).
39. S. Seung, *Connectome: How the Brain's Wiring Makes Us Who We Are* (Houghton Mifflin Harcourt, Boston, 2012).
40. N. Nagarajan, C. F. Stevens, *Curr. Biol.* **18**, R756 (2008).
41. K. Jezek, E. J. Henriksen, A. Treves, E. I. Moser, M. B. Moser, *Nature* **478**, 246 (2011).
42. T. J. Wills, C. Lever, F. Cacucci, N. Burgess, J. O'Keefe, *Science* **308**, 873 (2005).
43. J. Niessing, R. W. Friedrich, *Nature* **465**, 47 (2010).
44. F. Rosenblatt, *Psychol. Rev.* **65**, 386 (1958).
45. S. Haykin, *Neural Networks and Learning Machines* (Pearson Prentice-Hall, New York, 2009).
46. M. B. Goodman, D. H. Hall, L. Avery, S. R. Lockery, *Neuron* **20**, 763 (1998).
47. A. J. Whittaker, P. W. Sternberg, *BMC Biol.* **7**, 33 (2009).

Acknowledgments: H. Eckholdt played a key role in the early stages of this project. Contributions were also made by Z. Martirosyan, A. Singh, T. Stephney, and M. Zhang. C. Crocker made the figures. We thank J. White for encouragement and interest; A. Bergman, M. Chklovskii, D. Faber, A. Massimi, and S. Seung for helpful discussions; N. Baker, H. Buelow, D. Faber, R. Garcia, Z. Kaprielian, R. Lints, D. Portman, J. Sze, and J. Vijg for comments on the manuscript; and J. White and J. Hodgkin for their help in transferring archival transmission EM data from the U.K. Medical Research Council (MRC)–Laboratory of Molecular Biology to the Hall lab at Einstein for long-term curation and study. This work was supported by MRC, the U.S. NIH (R21MH63223 to S.W.E. and OD 010943 to D.H.H.), and by the G. Harold and Leila Y. Mathers Charitable Foundation.

Supplementary Materials

www.sciencemag.org/cgi/content/full/337/6093/437/DC1
Materials and Methods
Supplementary Text
Figs. S1 to S11
Table S1
References (*48*–*60*)
Movie S1
Databases S1 to S9

10.1126/science.1221762

REPORTS

Binary Interaction Dominates the Evolution of Massive Stars

H. Sana,[1]* S. E. de Mink,[2,3] A. de Koter,[1,4] N. Langer,[5] C. J. Evans,[6] M. Gieles,[7] E. Gosset,[8] R. G. Izzard,[5] J.-B. Le Bouquin,[9] F. R. N. Schneider[5]

The presence of a nearby companion alters the evolution of massive stars in binary systems, leading to phenomena such as stellar mergers, x-ray binaries, and gamma-ray bursts. Unambiguous constraints on the fraction of massive stars affected by binary interaction were lacking. We simultaneously measured all relevant binary characteristics in a sample of Galactic massive O stars and quantified the frequency and nature of binary interactions. More than 70% of all massive stars will exchange mass with a companion, leading to a binary merger in one-third of the cases. These numbers greatly exceed previous estimates and imply that binary interaction dominates the evolution of massive stars, with implications for populations of massive stars and their supernovae.

With masses larger than 15 times that of our Sun (*1*), stars of spectral type O are rare (*2*) and short-lived (*3*). Nevertheless, through their large luminosities, strong stellar winds, and powerful explosions, massive stars heat and enrich surrounding gas clouds in which new generations of stars form (*4*) and drive the chemical evolution of galaxies (*5*). Massive stars end their lives in luminous explosions, as core-collapse supernovae (CCSN) or gamma-ray bursts (GRBs), that can be observed throughout most of the universe.

In a binary system, the evolutionary path of a massive star is drastically altered by the presence of a nearby companion (*6*–*8*). Because stars expand as they evolve, those in pairs with orbital periods up to ~1500 days exchange mass (*6*). The more massive star can be stripped of its entire envelope and, thus, loses much of its original mass. The companion star gains mass and angular momentum, which trigger mixing processes in the stellar interior and modify its evolutionary path (*3*). In very close binaries, the two stars may even merge. The nature of the binary interaction is largely determined by the initial orbital period and mass ratio. The relative roles of interaction scenarios and the overall importance of binary- versus single-star evolution so far remain uncertain because of the paucity of direct measurements of the intrinsic distributions of orbital parameters (*9*–*14*).

In this work, we homogeneously analyze the O star population of six nearby Galactic open stellar clusters and simultaneously measure all the relevant intrinsic multiplicity properties (*15*). Our observational method, spectroscopy, is sensitive to orbital periods as long as 10 years (*13*), corresponding to the relevant period range for binary interaction (*6*). In a spectroscopic binary, the periodic Doppler shift of spectral lines allows the determination of the radial velocity and, hence, of the orbital motion of one ("single-lined" spectroscopic binary) or both ("double-lined" spectroscopic binary) stars. Given sufficient orbital-phase coverage, the orbital period (P), the eccentricity (e), and, for double-lined spectroscopic binaries, the mass-ratio (q) follow from Kepler's laws.

Our sample contains 71 single and multiple O-type objects (see supplementary text A). With 40 identified spectroscopic binaries, the observed binary fraction in our sample is $f_{obs} = 40/71 = 0.56$. We combined observations obtained with the Ultraviolet and Visible Echelle Spectrograph at the Very Large Telescope for long-period systems with results from detailed studies of detected systems in the individual clusters (*16*–*21*). In total, 85 and 78% of our binary systems have, respectively, constrained orbital periods and mass ratios. This allowed us to build statistically significant observed period and mass-ratio distributions for massive stars (Fig. 1), which are representative of the parameter distributions of the Galactic O star population (*13*).

The precise fraction of interacting O stars and the relative importance of the different interaction scenarios are determined by the distributions of the orbital parameters. The observed distributions result from the intrinsic distributions and the observational biases (see supplementary text B). To uncover the intrinsic distributions, we simulate observational biases with the use of a Monte Carlo approach that incorporates the observational time series of each object in our sample. We adopt power laws for the probability density functions of orbital periods (in $\log_{10}$ space), mass ratios, and eccentricities with exponents π, κ, and η, respectively (fig. S3 and table S3). These power-law exponents and the intrinsic binary fraction f_{bin} were simultaneously determined by a comparison of simulated populations of stars with our sample allowing for the observational biases. We determined the accuracy of our method by applying it to synthetic data.

Compared with earlier attempts to measure intrinsic orbital properties (*9*–*14*): (i) The average number of epochs per object in our sample is larger by up to a factor of 5, making binary detection more complete. (ii) More than

[1]Astronomical Institute Anton Pannekoek, Amsterdam University, Science Park 904, 1098 XH, Amsterdam, Netherlands. [2]Space Telescope Science Institute, 3700 San Martin Drive, Baltimore, MD 21218, USA. [3]Department of Physics and Astronomy, Johns Hopkins University, Baltimore, MD 21218, USA. [4]Astronomical Institute, Utrecht University, Princetonplein 5, 3584 CC, Utrecht, Netherlands. [5]Argelander-Institut für Astronomie, Universität Bonn, Auf dem Hügel 71, 53121 Bonn, Germany. [6]UK Astronomy Technology Centre, Royal Observatory Edinburgh, Blackford Hill, Edinburgh EH9 3HJ, UK. [7]Institute of Astronomy, University of Cambridge, Madingley Road, Cambridge CB3 0HA, UK. [8]Fonds de la Recherche Scientifique—FNRS, Institut d'Astrophysique, Liège University, Allée du 6 Août 17, B-4000 Liège, Belgium. [9]Université Joseph Fourier–Grenoble 1/CNRS–Institut National des Sciences de l'Univers, Institut de Planétologie et d'Astrophysique de Grenoble UMR 5274, Grenoble, France.

*To whom correspondence should be addressed. E-mail: h.sana@uva.nl

The Connectome of a Decision-Making Neural Network

Travis A. Jarrell, Yi Wang, Adam E. Bloniarz, Christopher A. Brittin, Meng Xu, J. Nichol Thomson, Donna G. Albertson, David H. Hall, and Scott W. Emmons

Science, 337 (6093), • DOI: 10.1126/science.1221762

The Male Wiring Diagram

The function of the nervous system is thought to represent an emergent property of its network connectivity. However, there are few complete descriptions of all the physical connections between neurons within a real nervous system. Working in nematodes, Jarrell *et al.* (p. 437; see the Perspective by Chklovskii and Bargmann) identified the complete connectome—every single chemical and gap junction synapse—of the tail ganglia, which govern mating behavior.